156
12-23-75

OR-1863

UCRL-51919

THE EFFECT OF STRESS ON THE MICROSTRUCTURE OF A GRAYWACKE SANDSTONE FROM THE SITE OF THE RIO BLANCO GAS-STIMULATION EXPERIMENT

L. A. Dengler

September 30, 1975

Prepared for U.S. Energy Research & Development Administration under contract No. W-7405-Eng-48

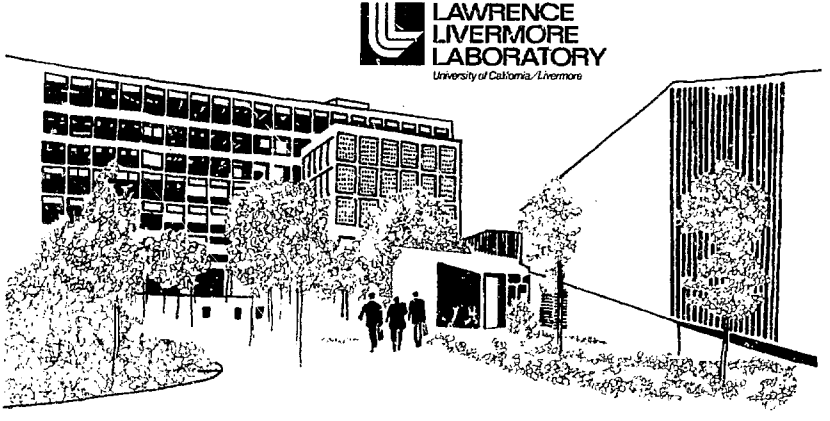

Printed in the United States of America
Available from
National Technical Information Service
U. S. Department of Commerce
5285 Port Royal Road
Springfield, Virginia 22151
Price: Printed Copy $___*; Microfiche $2.25

*Pages	NTIS Selling Price
1-50	$4.00
51-150	$5.45
151-325	$7.60
326-500	$10.60
501-1000	$13.60

Distribution Category
UC-4

LAWRENCE LIVERMORE LABORATORY
University of California/Livermore, California/94550

UCRL-51919

THE EFFECT OF STRESS ON THE MICROSTRUCTURE OF A GRAYWACKE SANDSTONE FROM THE SITE OF THE RIO BLANCO GAS-STIMULATION EXPERIMENT

L. A. Dengler

MS. Date: September 30, 1975

Contents

THE EFFECT OF STRESS ON THE MICROSTRUCTURE OF A GRAYWACKE SANDSTONE FROM THE SITE OF THE RIO BLANCO GAS-STIMULATION EXPERIMENT

Abstract

Unstressed and laboratory-stressed samples of graywacke sandstone from the site of the Rio Blanco gas-stimulation experiment were studied, both optically and with a scanning electron microscope, to relate imposed stress to pore and microcrack structure. This sandstone consisted of 100-300-μm-diameter clasts (principally quartz and feldspar) in a fine-grained (<10 μm diameter) matrix of clay and cementing minerals. The porosity of the rock was contained in tortuous networks of narrow (<10 μm diameter) channels around and between cement grains. Samples deformed in both uniaxial-strain and uniaxial-stress experiments were studied. The microscopic effects of uniaxial-strain conditions were occasional short (<0.5 grain diameter) transgranular fractures, partial cement breakdown, and narrow cracks at the grain boundaries. Increased strain appeared to increase the degree of fracturing. The effects of uniaxial-stress conditions varied with the confining pressure of the test. Macroscopic brittle behavior (one or two throughgoing fault zones) was observed in samples tested at confining pressures of less than 50 MPa. Microscopically, fracture in brittle samples was principally restricted to grain boundaries, with transgranular fractures observed only along the immediate fault. Away from this zone, clasts were unfractured, although the cement matrix was partially broken down. On the fault surface of brittle samples there was little gouge or striation, implying little friction during failure. Transitional behavior (macroscopic barreling of sample, recognizable shear zones) was exhibited by samples tested under confining pressures between 50 and 500 MPa. Transgranular fractures were observed throughout transitional samples, although their occurrence was highly concentrated in the vicinity of the fault zone. With the exception of the shear zone, these fractures rarely extended further than a grain diameter. On the shear surface, transitional samples showed a rubble-like appearance, with broken grain and cement fragments intermixed, indicative of frictional sliding on this surface. Macro-

scopic ductile behavior (barreled, no continuous shear zone) was observed in a sample tested at 600 MPa confining pressure. Extensive fracturing, consistently extending many grain diameters in length, was characteristic of the ductile sample. Fractured and striated grains and cement gouge were observed throughout the sample, indicating widespread frictional sliding.

Introduction

Project Rio Blanco was designed to increase rock permeability in an existing gas reservoir by fracturing the rock with a vertical array of three simultaneous nuclear explosions. The project site was CER Geonuclear hole RB-E-01, Section 14, T35, R98W, Rio Blanco County, in the Piceance Creek Basin of northwest Colorado. General information regarding the project and the reservoir rock is given in Refs. 1 and 2.

The most essential part of this project was to produce fracturing in, and thereby to increase the permeability of, the reservoir rock. This report contains the results of optical and scanning electron microscope (SEM) studies done on unstressed and laboratory-stressed samples of graywacke sandstone from the 6458-ft level of the emplacement hole. Laboratory-stressed samples were from uniaxial-stress and uniaxial-strain tests made as part of equation-of-state measurements used to provide input parameters for preshot code calculations. The purpose of this study is to examine specimens from controlled tests on laboratory samples. It is intended eventually to relate these results to microscopic studies being done on postshot cores.

Experimental Procedure

All samples discussed here are from the 6458-ft horizon of the Cretacious Mesa Verde Formation; they are characterized by a bulk density of 2.491 Mg/m^3, a grain density of 2.661 Mg/m^3, and a total porosity of 6.8%. Details of the laboratory experiments are described elsewhere.[3] Polished thin sections were used for optical microscopic studies made with both transmitted and reflected light. The laboratory-stressed samples were first coated with epoxy resin to keep them intact, then sliced along their lengths and through their centers to make axial and radial sections. Sections were ground with 6-μm Al_2O_3 abrasive on a brass-alloy lap and polished with a 0.5-μm diamond-powder abrasive. Kerosene was used as a lubricant throughout, in an attempt to avoid altering the clay mineral structure. The remainder of the sample was used to obtain specimens for SEM studies. Where faults were formed, the fault surface was used as the specimen surface. To study intact samples or regions away from the fault zone, specimens were made by tension failure (bending) of the sample. This method of sample preparation was chosen to minimize artifacts produced by grinding and polishing. Although clay fabric is especially susceptible to damage during specimen preparation, extremely delicate networks and bridges of cement matrix were observed intact (see Figs. 6, 7, and 21), showing this method to leave much of the sample undisturbed. The only further specimen preparation consisted of either treatment in an ultrasonic cleaner or blowing with compressed air to remove loose dust fragments from the surface, and the evaporation of a 10-20-nm layer of gold-palladium alloy over the specimen to provide a conducting surface for SEM operation.

A Coates & Welter Field Emission Scanning Electron Microscope with maximum resolution of 6 nm in the emissive mode was used in this study. An x-ray energy spectrometer (microprobe) attachment to the SEM was used for mineral identification.

Optical studies[4] have been made on similar graywacke-type sandstones from laboratory-stressed samples. However, it is impossible to observe cement structure and microporosity with the optical microscope, as its maximum resolving power is limited by the wavelength of light to around 300 nm. It is also difficult to distinguish fractured from unfractured

grain boundaries with the optical microscope. The microporosities of several sedimentary rocks have been studied with the SEM,[5-7] but these studies did not include stressed samples.

Observations

UNSTRESSED ROCK

Optical studies of unstressed material showed angular grains of quartz, feldspar, and occasional calcite and other rock fragments (diameters between 100 and 300 μm) in a cement matrix (Fig. 1). The clasts appeared unfractured. Details of the cement matrix and pore structure could not be seen. It was impossible to determine if fractures occurred along grain boundaries.

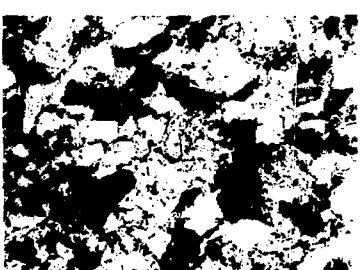

Fig. 1. Optical photomicrograph of unstressed Rio Blanco graywacke sandstone from the 6458-ft horizon of hole RB-E-01.

Under the SEM, the same sample appeared quite different from the optical section. At low magnification it appeared as an alternation of smooth and rough surfaces, with individual grains difficult to distinguish (Fig. 2). At higher magnification, with use of a microprobe, the smooth areas were identified as the surfaces of quartz grains. The cement material seemed to adhere less strongly to the quartz grains than the other constituents of this rock, leaving "clean" quartz surfaces when the sample was fractured.

Many of the quartz grains were also characterized by numerous, small (<1 μm diameter) pits, as shown in Fig. 3. These pits are most likely a result of grain transportation and deposition (a detailed SEM study of detrital quartz grain-surface textures is given by Krinsley and Margolis[8]), and probably do not add to the interconnected pore structure and permeability of the rock.

The rough areas in Fig. 2 are generally feldspar grains in various stages of alteration. The roughness

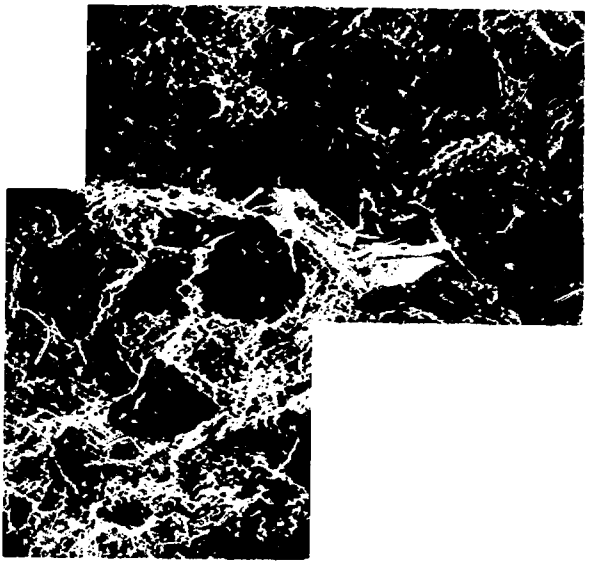

Fig. 2. Low-magnification SEM photomicrograph of unstressed rock (ultrasonically cleaned specimen). "Smooth" areas are quartz grains; "rough" surfaces are generally feldspar or other rock fragments. The arrow points to the grain boundary enlarged in Fig. 7.

is caused by a "hairy" coat of clay and cement (Fig. 4). In some cases, as shown in Fig. 5, the clay minerals appear to be emerging out of the grain surface. At high magnification, the intricacies of matrix and pore structure can be observed with the SEM. Figure 6 shows some of the crystal forms making up the matrix. Because of their extremely small size (generally less than 10 μm in length and often less than 1 μm in thickness), their mineralogy cannot be resolved with a microprobe. Figure 7 is a higher magnification view of a grain boundary in Fig. 2. The intergranular area is seen to be full of cement material (principally clay-mineral

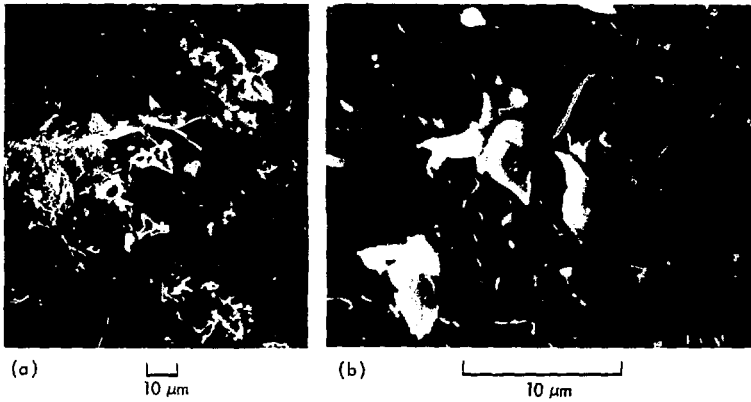

Fig. 3. (a) Isolated quartz grain from unstressed rock. The small particles adhering to the surface are broken cement grains. (b) Detail of the "pitted" end of the grain.

crystals in this figure). The delicate structure of these crystals indicates that specimen preparation has left this area undisturbed. The porosity can be seen in the void spaces around and between the cement structure. The "average" pore is angular in shape and less than 10 μm in width (Fig. 8). The measured low gas permeability[9] of the sandstone is probably caused by the small average pore size and the sinuosity of the pore network.

UNIAXIALLY STRAINED SAMPLES

In the uniaxial-strain experiment, axial stress (σ_1) was increased under the condition that the radial strain remain constant. This loading path is thought to represent the passage of a plane shock wave, strain not being allowed normal to the direction of wave propagation.[10] Table 1 tabulates stress-strain data on samples used in this study.

Figure 9 is an optical photomicrograph from RB 62. Compared with those in the unstressed sample (Fig. 1), clasts in the stressed sample appear somewhat closer together. A few short (<0.5 grain diameter) transgranular fractures can be seen. There were no noticeable areas of fracture concentration throughout the axial section except some near the ends of the sample cylinder, probably reflecting stress concentrations due to end effects caused by the piston.

Fig. 4. (a) Portion of feldspar grain in unstressed rock. The slightly curving edge in the upper part of the photomicrograph is the grain boundary. Most of the grain surface is obscured by cement and matrix material. The area indicated by the arrow is enlarged in Fig. 4b. (b) Detail of matrix (indicated by arrow in Fig. 4a).

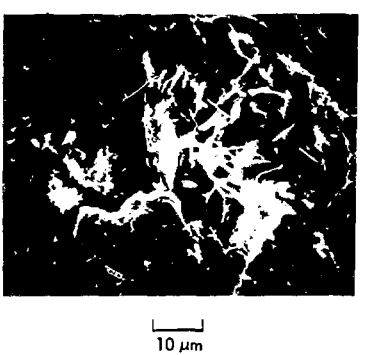

Fig. 5. Isolated feldspar grain in unstressed rock. The arrow points to an area where clay minerals appear to be emerging from the grain surface.

Figure 10 compares photomicrographs taken from near the central areas of axial sections of each of the samples studied. No pronounced difference between RB 62 and RB 9 was found in the otpical investigation. Qualitatively, RB 65 appears to show greater incidence of grain fracturing and compaction (clasts moved closer together). The microscopic differences do not seem pronounced enough to predict percentage strain by degree of sample response to stress.

Under the SEM, at low magnification, these samples appear different from the unstressed samples (compare Figs. 11 and 2). Individual grains are more easily distinguished in the stressed than in the unstressed rock.

Fig. 6. High-magnification photomicrographs showing some of the crystal forms seen in the matrix of unstressed rock (ultrasonically cleaned specimen).

Grains appear closer together, in agreement with optical findings. In addition to overall sample compaction, the bulk of the specimen seems more weakly consolidated than the unstressed rock.

At high magnification the differences between stressed and unstressed rock become more pronounced. As in the optical studies, short (<0.5 grain diameter) transgranular fractures can be seen. In the optical photomicrograph (Fig. 9), transgranular fractures appear as dark hairline traces on the background of the clast. The SEM (Fig. 12) reveals the shape, width, and, to some degree, depth of these cracks. The crack tips often appear blunt or square, and less than 5 μm in width. The following observations suggest that these cracks are probably new: no similar cracks are observed in the unstressed rock; the cracks are free of clays and cement, which seem to fill any opening in this rock; and the crack surfaces appear sharp and clean, with offsets easily observable. Very narrow cracks (<1 μm wide) can also be seen in Figs. 12b and 12c.

The major difference between uniaxial-strain samples and unstressed rock may be seen at the grain boundaries. In the unstressed sample (Fig. 7), the intergranular areas are filled with clay networks and cement matrix. Figure 13 is an enlargement

Fig. 7. Detail of grain boundary shown in Fig. 2. The intergranular area is filled with matrix material, principally clays in this photomicrograph. The porosity of the rock is contained in the open spaces around and between the matrix structure.

Table 1. Maximum attained values of axial stress (σ_1), confining pressure (σ_3), differential stress [$\tau = (\sigma_1 - \sigma_3)/2$], and longitudinal strain for triaxial-strain tests.

Sample	σ_1 (MPa)	σ_3 (MPa)	τ (MPa)	Strain[a] (%)
RB 62	490.7	300.6	95.1	-1.4
RB 9	951.2	695.7	77.7	-2.5
RB 65	1032.1	684.5	173.8	-3.3

[a]Strains are negative in compression.

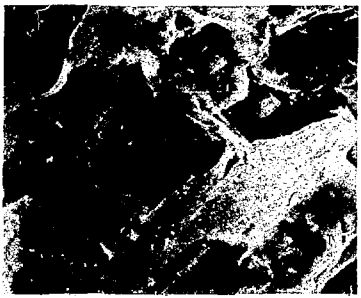

Fig. 8. Detail of pore between clay minerals in unstressed rock (ultrasonically cleaned specimen).

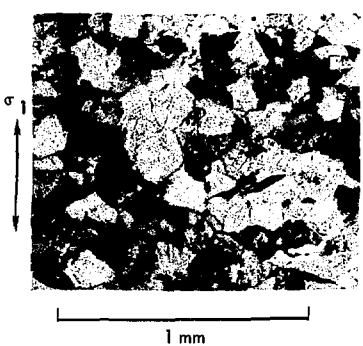

Fig. 9. Optical photomicrograph of sample RB 62, tested under conditions of uniaxial strain. The axis of maximum principal stress (σ_1) is indicated. Note the short transgranular cracks, which are not seen in the unstressed sample (Fig. 1).

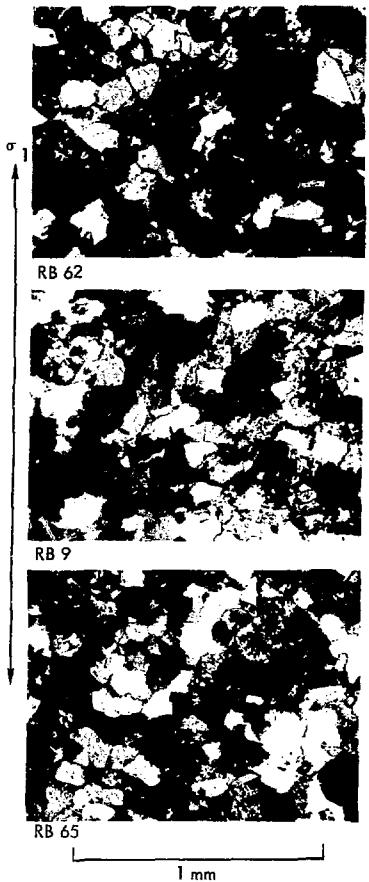

Fig. 10. Photomicrographs from axial sections of RB 62, RB 9, and RB 65, made with doubly polarized light. The axis of maximum stress (σ_1) is indicated. Grain fracturing appears most pronounced in RB 65.

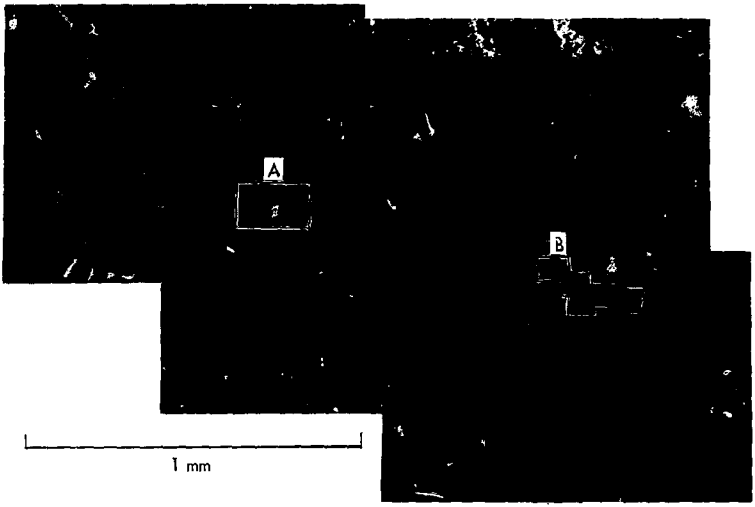

Fig. 11. Tensile fracture surface from RB 62 (ultrasonically cleaned specimen). Compared with unstressed sample (Fig. 2), the clasts appear more distinct. Region A is the grain boundary enlarged in Fig. 12; region B is the grain boundary enlarged in Fig. 13.

of a grain boundary from Fig. 11. This specimen shows many places which are virtually free of cement. Narrow (<1 μm wide), continuous grain-boundary cracks are also seen. Both this specimen and the unstressed specimen were treated in an ultrasonic cleaner which removed any broken cement fragments. This treatment cannot be responsible for initially breaking down the cement structure, as the cement is intact in an unstressed sample given the same treatment (Fig. 7). There are areas within the same specimen in which the cement appears undisturbed (Fig. 13b).

The above discussion refers to SEM investigation of RB 62, the sample tested at the lowest strain and differential stress of the three samples studied. RB 9 showed similar microscopic behavior, and, as in the optical study, differences between RB 62 and RB 9 could not be seen. RB 65 showed similar grain-

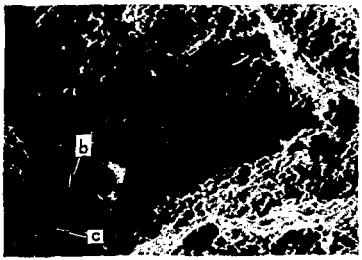

Fig. 12. (a) Enlargement of region A in Fig. 11. The arrows point to short transgranular cracks enlarged in (b) and (c).

boundary behavior but larger (in length and width) and more frequent grain fracturing than the other two samples.

In summary, uniaxial-strain samples showed some microscopic features not seen in the unstressed rock. Even at the lowest maximum sample strain (1.4%), grains appeared closer together (causing sample compaction) and showed short transgranular fractures. The cement matrix was partially broken down, and narrow grain-boundary cracks were seen. Increased differential stress appeared to increase specimen damage (grain-boundary and cement fracturing), but differences were pronounced only in the sample strained to 3.3%.

UNIAXIALLY STRESSED SAMPLES

In uniaxial-stress experiments, the least and intermediate principal stresses are kept equal and constant (referred to as confining pressure or σ_3). The axial stress (σ_1) is increased until failure occurs. If a sample achieves 5% or more permanent strain prior to failure, its behavior is arbitrarily termed ductile. Brittle failure is characterized by lack of permanent strain, and intermediate behavior is called transitional (these definitions are discussed by Griggs and Handin[11] and

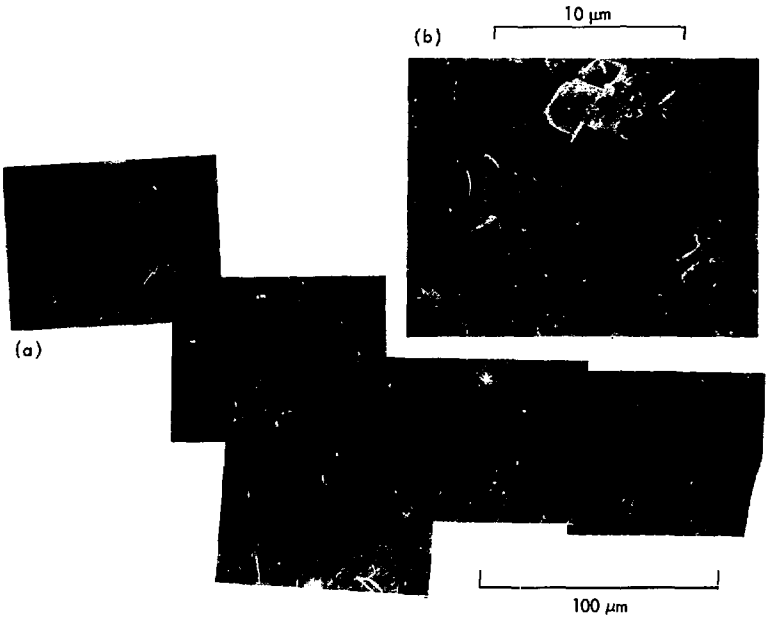

Fig. 13. (a) Enlargement of region B in Fig. 11. Note the absence of intergranular material and the occurrence of narrow grain-boundary cracks. The arrow points to the area enlarged in (b), where clay-mineral crystals are undisturbed.

Schock et al.[12]). These behavior regimes are based on stress-strain observations, but also correspond to distinct differences in microstructure as discussed by Borg[4] in a study on laboratory-deformed graywacke sandstones from the Wagon Wheel Project emplacement hole.

Stress-strain information on the samples used in the uniaxial-stress experiments is given in Table 2. For these samples, brittle failure occurred at less than 50 MPa confining pressure, ductile failure at over 500 MPa, and transitional failure at intermediate confining pressures (50-500 MPa).

Macroscopically, brittle samples were broken roughly in half by one or two throughgoing faults, extending diagonally the length of the sample cylinder. Optical photomicrographs

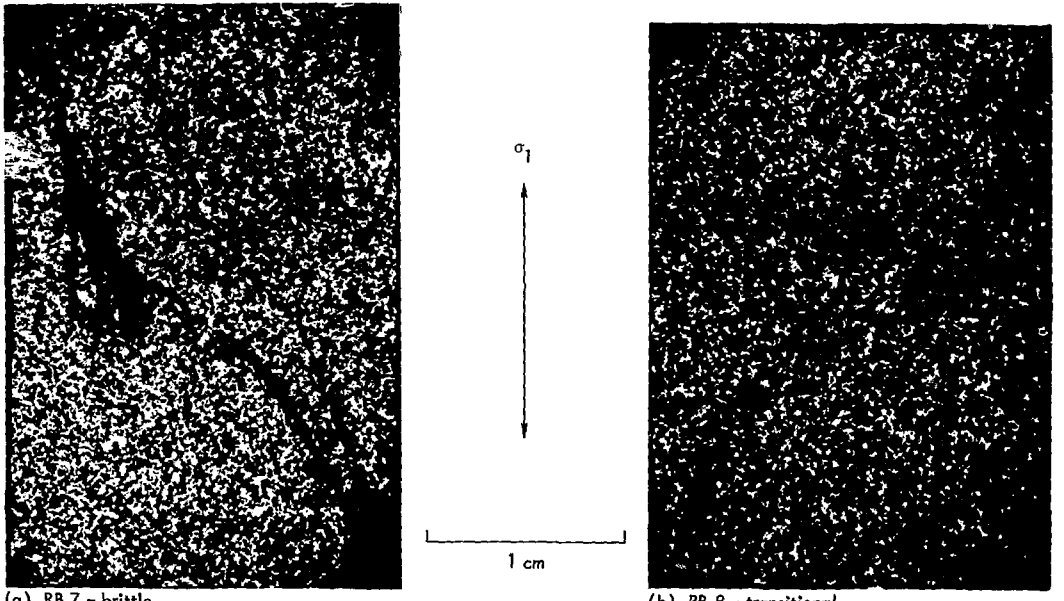

Fig. 14. Axial sections from three uniaxially stressed samples (photographed with doubly polarized light). Each photomicrograph is of a longitudinal plane, parallel to the axis of maximum principal stress (σ_1). (a) RB 7, 0.1 MPa confining pressure. Brittle behavior: note the well-defined fault zone; failure occurred mainly at grain boundaries, with the bulk of the sample appearing undisturbed. Compare with unstressed rock in Fig. 14d. (b) RB 8, 100 MPa confining pressure. Transitional behavior: note the shear zone and barreling of the sample; transgranular failure is predominant on the shear zone and is seen occasionally throughout the sample.

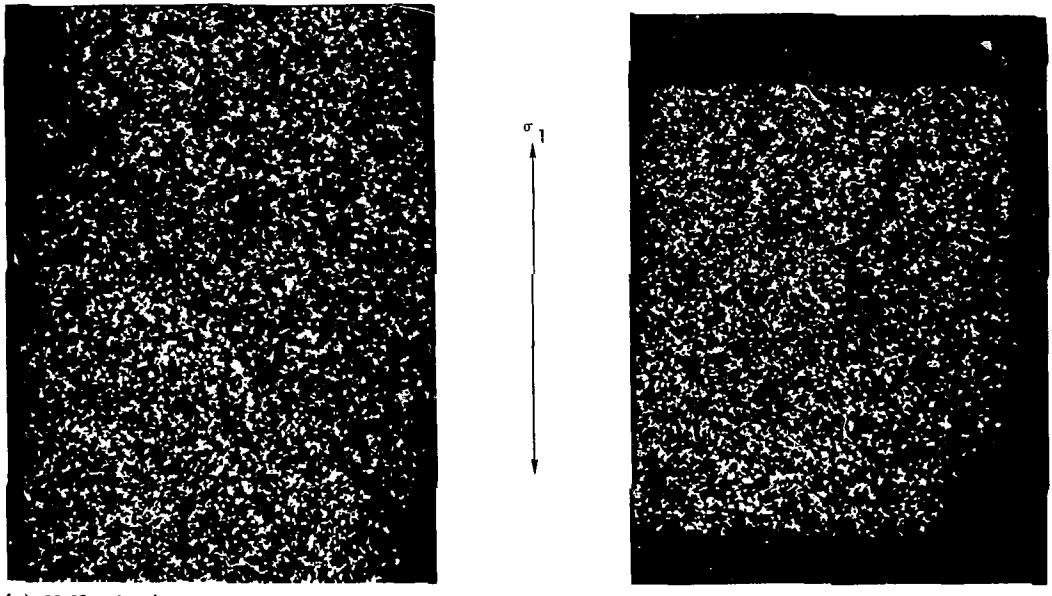

Fig. 14 (continued). (c) RB 12, 600 MPa confining pressure. Ductile behavior: note the poorly defined shear zone, barreling of the sample, and frequent occurrence of transgranular fracture throughout the sample. (d) Unstressed rock.

Table 2. Maximum attained values of axial stress (σ_1), confining pressure (σ_3), differential stress [$\tau = (\sigma_1 - \sigma_3)/2$], and radial and longitudinal strains from uniaxial-stress tests.

Sample	σ_1 (MPa)	σ_3 (MPa)	τ (MPa)	Radial strain[a] (%)	Longitudinal strain[a] (%)
RB 7	76.5	0.1	38.2	0.56	- 0.5
RB 10[b]	72.6	0.1	31.3	0.6	- 0.47
RB 4	230.1	40	95.1	1.46	- 1.49
RB 8	314.2	100	107.1	3.79	- 2.59
RB 11[b]	537.2	300	118.6	2.9	- 5.70
RB 12	872.3	600	136.2	5.5	- 4.47

[a]Strains are negative in compression.

[b]RB 10 and RB 11 were partially loaded, unloaded, and then reloaded to failure.

show failure occurring predominantly at grain boundaries (Fig. 14a). The few transgranular fractures that were seen were restricted to the immediate zone of failure. Away from this zone the sample appears indistinguishable from the unstressed rock (Fig. 14d).

The transitional samples were barreled (this can be seen in the slight curvature of the cylinder outline in Fig. 14b, differing from the straight cylinder profile of Fig. 14a). As in the brittle regime, the cylinders were separated into two pieces by throughgoing shear fractures. The mode of failure differed from the brittle mode by a predominant occurrence of transgranular fracture (Figs. 14c and 15a). Grains in the shear zone were broken into small fragments. Some transgranular fractures were seen throughout the bulk of the sample, although grain fracturing was concentrated near the shear zone. Figure 15 compares a photomicrograph of an unstressed sample with photomicrographs of a transitional sample, both on the failure zone and away from it.

The only sample studied that failed in the ductile regime (RB 12, tested at 600 MPa confining pressure) was macroscopically barreled and wholly intact (no well-defined shear zone truncating the sample). The optical section (Fig. 14c) shows

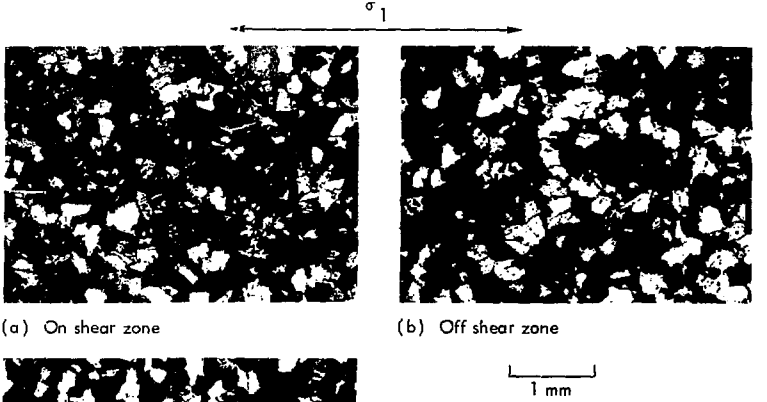

Fig. 15. (a) Photomicrograph of axial section of transitional sample RB 8 (100 MPa confining pressure) along failure zone (photographed with doubly polarized light). (b) Same sample as Fig. 15a; away from shear zone. (c) Unstressed sample.

virtually no shear zone. Extensive grain fracturing was observed throughout the sample, differing from the noticeable concentration of transgranular fracturing near the shear zone as seen in samples tested at lower confining pressures.

SEM studies made on the above samples concentrated on grain boundaries, cement matrix, pore structure, and the size and shape of transgranular fractures - subjects inaccessible to the optical microscope. Specimens were taken at the shear-zone surfaces and away from this zone for samples in all three behavior regimes (specimens were examined from several areas of RB 12, which exhibited no distinct fault zone and hence no single shear surface).

Figure 16 is a low-magnification photomicrograph of the fault surface of brittle sample RB 7. The brittle failure plane is characterized by

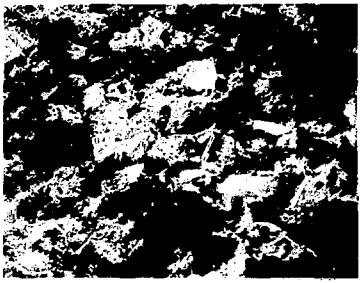

Fig. 16. SEM photomicrograph of the failure surface of RB 7. Note the frequency of grain-boundary cracks and rare occurrence of transgranular cracks. (Air-blown only; no ultrasonic treatment.)

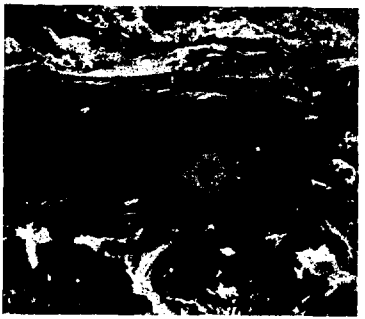

Fig. 17. Failure surface of RB 7 (same specimen as Fig. 16): conchoidal fracture in quartz clast. Note absence of striations or gouge, indicating an absence of frictional sliding along this surface. Also note the small pits (similar to those seen in Fig. 3) on the side of the grain.

loosened grains and surrounded by fairly wide (up to 10 μm) grain-boundary cracks. These cracks should greatly increase the pore size on this plane. Along the fault plane, clasts are mainly unfractured, although some fresh conchoidal fracture surfaces (indicating a broken quartz clast) are seen (Fig. 17). There was little gouge (broken grain and cement fragments) or other evidence indicating much frictional sliding on the failure surface. Breakdown of matrix structures accompanied grain-boundary fractures on the failure surface. In Fig. 18, the grains appear pulled apart, with the cement networks broken. In several places the cement minerals have a "stringy" appearance. No similar mineral forms were seen in the cement matrix of the unstressed rock. This may be an altered form of a clay or matrix mineral possibly due to frictional heating or stress during deformation. Specimens from the same sample taken away from the failure zone appeared markedly similar to uniaxially strained samples RB 62 and RB 9 - i.e., no major transgranular fractures, narrow grain boundary cracks, and some broken cement, although much of the cement and clay

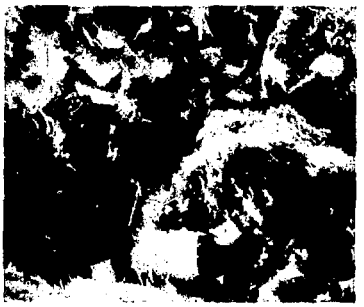

Fig. 18. (a) Detail of grain boundary structure of shear zone surface of RB 7 (air-blown only; no ultrasonic treatment). The clay and cement structure appears pulled apart. (b) Enlargement of Fig. 18a: note the "stringy" form of the matrix material.

structure was undisturbed, as shown in Fig. 19. No similar expanses of undisturbed clays were observed in samples tested at confining pressures of more than 50 MPa.

The failure surface of a transitional sample is shown in Fig. 20. Transgranular and grain-boundary fracturing was far more extensive than on the corresponding surface in a brittle sample (compare Fig. 20 with Fig. 16). The broken grain and cement gouge on this surface indicate some frictional sliding along the fault plane during or after failure. The intergranular areas along the failure surface (filled with dense networks of clay and cement minerals in the unstressed sample; see Figs. 6 and 7)

Fig. 19. Undisturbed clay minerals in cement matrix of RB 7 away from failure zone.

Fig. 20. Failure surface of transitional sample RB 8((air-blown only; no ultrasonic treatment). The arrow points to the area enlarged in Fig. 21.

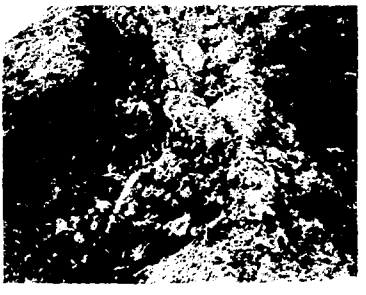

Fig. 21. Detail of broken grain and cement debris filling intergranular area of sample RB 8 indicated in Fig. 20.

were filled with broken grain fragments and cement debris (Fig. 21). Away from the shear zone, some transgranular fracturing was observed, in agreement with the optical findings. Fracturing on several scales can be seen in Fig. 22, a micrograph of a quartz clast in RB 11. The main fracture in this grain is about a micrometer wide, and the smallest is an order of magnitude less. The fractures in this grain were restricted to the length of the grain. Rarely were transgranular fractures (from specimens off the shear zone) observed to extend further than one grain diameter in transitional samples. The cement matrix appeared to have acted as a "sponge," effectively damping out crack propagation. Although grain-boundary fractures frequently occurred away from the shear zone, they were usually limited to the length of a single grain (Fig. 23).

Specimens were taken from several areas of the ductile sample RB 12 for SEM study. All specimens showed massive fracturing of all components of the rock system. Figure 24 (from a section away from the center) shows an example of the degree of fracturing present in this sample. In brittle and transitional samples, fractures away from the shear zone were rarely observed to extend longer than a single grain diameter. The fracture shown in Fig. 24 extended at least

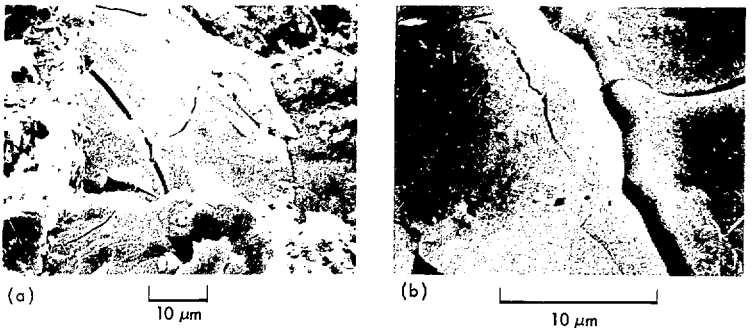

Fig. 22. (a) Region away from the failure zone of transitional sample RB 11 (air-blown only; no ultrasonic treatment), showing transgranular fractures in a quartz clast. (b) Detail of Fig. 22a. Note the various sizes of cracks in the same grain. The "pits" seen in this grain appear dissimilar to those seen in Figs. 3 and 8 and are likely to have a different origin, possibly being the remains of fluid inclusions.

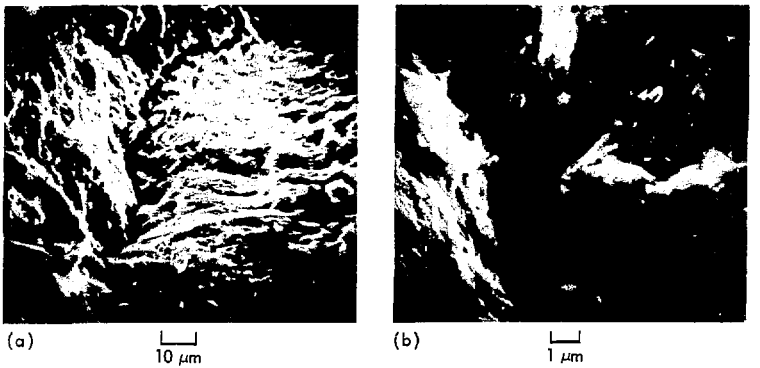

Fig. 23. (a) Grain boundary fracture in RB 8, away from shear zone (ultrasonically cleaned specimen). (b) Detail of Fig. 23a.

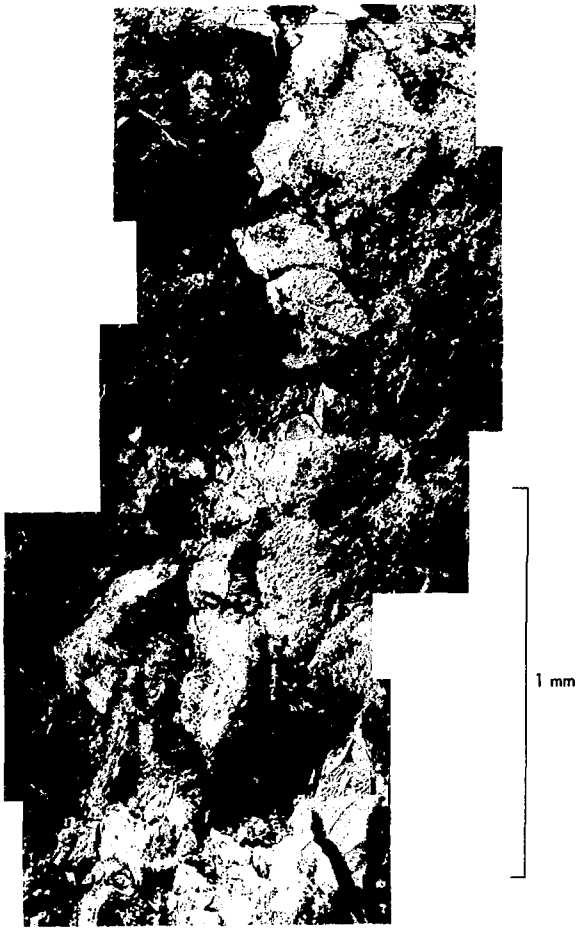

Fig. 24. Ductile sample RB 12, away from incipient shear zone (air-blown only; no ultrasonic treatment). The fracture is a continuous system of interconnected transgranular and intergranular cracks.

the length of about 12 grains, with transgranular and grain-boundary cracks linking up to form a continuous system. The specimen surface also showed broken grain and cement gouge, indicating frictional sliding throughout the sample. This is consistent with the >5% permanent strain achieved in the sample prior to failure. At 600 MPa confining pressure, the "sponge" effect of the cement matrix appears to have been overcome, allowing the hard components of the system (the clasts) to be in sufficient contact to fracture continuously. The plasticity of the clays and cement is still critical to the system, however, allowing material components to move relative to each other to cause the permanent strain recorded. When studied at higher magnification, single grains were often observed to have several throughgoing fractures that tended to be aligned nearly parallel to the axis of maximum stress (Fig. 25); similar findings were reported by Borg et al.[13] in a study of deformed St. Peter sand. Cement minerals appeared to be broken down or pulled apart at every grain boundary (Fig. 26), so that the entire cement matrix was effectively destroyed. The "stringy" form of cement minerals was frequently observed in this sample, possibly a response to stress. Microscopic observations made on the uniaxially stressed samples are summarized in Table 3.

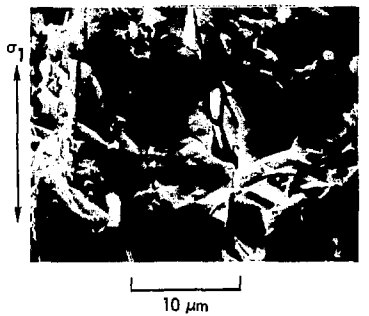

Fig. 25. Transgranular fractures in quartz grain of RB 12. The axis of maximum principal stress (σ_1) is indicated.

Fig. 26. Grain-boundary area of RB 12. Note the "stringy" habit of the matrix material.

Table 3. *Uniaxial-stress tests* — summary of behavior.

Sample	Mechanical Behavior	Macroscopic description of sample	Optical observations	SEM observations
RB 7	Brittle	Single fault	Fault: discontinuous at center of specimen. Failure along grain boundaries, transgranular fracture rare and restricted to shear plane. Bulk of specimen appears undeformed.	On fault zone: grains loosened, with extensive grain-boundary cracks. Cement structure between grains generally broken down. Fresh fracture surfaces on some grains, indicating transgranular fracture. No evidence of frictional sliding on shear plane. Off fault zone: Intact grains, partially disturbed cement, and narrow grain-boundary cracks.
RB 10	Brittle	Two conjugate faults	Two fault zones. Failure principally at grain boundaries, but greater incidence of transgranular fracturing. This fracturing concentrated in center of sample and appeared to be aligned along axis of maximum stress.	Not studied
RB 4	Brittle	Single shear plane	Continuous fault. Several subsidiary faults near center of sample aligned parallel to maximum stress axis, ~4 mm long. Failure principally along grain boundaries, but transgranular fractures occurring more often than in RB 7 and in a wider zone about the fault plane.	On shear zone: Fracturing more extensive than in RB 7, giving indication of some frictional sliding. Transgranular fractures frequent cement structure broken down.

Table 3. (continued).

Sample	Mechanical Behavior	Macroscopic description of sample	Optical observations	SEM observations
RB 8	Transitional	Cylinder is barreled, single shear zone	Fault zone with offset features indicating relative displacement between the two sides. Failure predominantly transgranular, with grains in vicinity of shear plane highly broken up. Grain fractures occur throughout sample but occur most frequently near the failure zone.	On shear zone: Extensive grain, grain-boundary, and cement fracturing. "Gouge" appearance, indicating frictional sliding. Intergranular areas filled with broken grain and cement debris. Off shear zone: Frequent grain-boundary fracture and occasional transgranular fractures, limited in length to the grain diameter.
RB 11	Transitional	Same as RB 8	The general appearance of this sample is basically the same as RB 8. The zone of "demolished" grains on the shear zone is wider, and the occurrence of transgranular fractures off the shear zone is more frequent.	Observations essentially the same as for RB 8. Cement structure throughout the sample is broken down.
RB 12	Ductile	Cylinder barreled and intact — no shear zone	Extensive transgranular fracturing throughout sample, tending to be aligned parallel to maximum stress axis. Degree of fracturing throughout sample relatively uniform.	Long, continuous fractures (>10 grain diameters) throughout sample. Highly fractured grains and total breakdown of cement matrix.

Conclusions and Summary

In general the samples tested under conditions of uniaxial stress exhibited more fracturing than those that underwent uniaxial-strain deformation. It is important to note some inherent differences between these two test conditions. The maximum differential stress $\tau = (\sigma_1 - \sigma_3)/2$, and the maximum strain, at the same confining pressure, are always lower under conditions of uniaxial strain than under those of uniaxial stress. Samples tested in uniaxial strain never failed, while all of those in uniaxial stress were tested to failure. Schock and Heard[14] have shown that the condition of constant radial strain in a uniaxial-strain test appears to preclude the onset of dilatancy (inelastic volume changes thought to be caused by the opening of axially aligned microcracks). Dilatancy is believed to be a necessary precursor of brittle failure in rock.[15] It is interesting to note that, away from the shear zone in brittle samples RB 7 and RB 4 (uniaxial stress; 38.2 and 95.1 MPa differential stress, respectively), the samples appeared very similar to samples RB 62 and RB 9 (uniaxial strain; 95.1 and 77.7 MPa differential stress, respectively). Dilatancy is supposedly absent from uniaxially strained samples such as RB 9; dilatancy occurred in uniaxially stressed sample RB 7 (as measured by positive volumetric strains). The only significant microstructural difference between RB 9 and RB 7 was the occurrence of a fault in RB 7. With the exception of the fault zone, the samples were remarkably similar in appearance. This might indicate that dilatancy is occurring principally in the vicinity of the fault zone, i.e., that it is localized along the plane of eventual failure. Scholz,[16] in laboratory compression tests, found a clustering of microfracturing events (presumed to be the cause of dilatancy) along the eventual failure zone at over 90% fracture stress. At low confining pressures, it may be that dilatancy, as well as failure, is a local phenomenon.

Uniaxial-stress loading was effective in fracturing this rock. At low confining pressures, the main effect was the creation of narrow, throughgoing faults. Near these faults, grain-boundary cracks generally occurred, probably increasing both the average pore size and the number of interconnected pore networks. Away from the fault zone, the only observed effect of stress on the sample was the partial breakdown of

cement structure and the creation of some narrow grain-boundary cracks. Both of these processes could increase pore size, though certainly not to the extent occurring near the fault zone. As confining pressure was increased, the degree of fracturing throughout the sample also increased: i.e., the effect of confining pressure was to increase the degree of participation of all the grains in the failure process. At confining pressures below the ductile range, transgranular fracturing (away from the shear zone) was limited to the dimensions of a single grain and therefore would not be likely to create any significant new interconnected pore networks. At confining pressures in the ductile range, failure in the sandstone was accompanied by massive, well-distributed fracturing on all scales, which probably increased pore size and pore networks throughout the sample.

It is interesting to compare the behavior of this graywacke sandstone (a clastic sedimentary rock) with a granodiorite (holocrystalline igneous rock) tested in the same apparatus at the same confining pressure (300 MPa). Figure 27 compares axial sections from RB 11 and a uniaxially stressed sample of Piledriver granodiorite P16. Laboratory tests on Piledriver samples are described by Schock et al.[12]; pertinent data on P16 are: maximum principal stress = 886 MPa, differential stress = 293 MPa, radial strain = 1.0%, longitudinal strain = -1.7%. The photomicrographs in Fig. 27 were taken from similar locations, away from the shear zone. The significant mechanical difference between the graywacke and the granodiorite is the amount of strain at failure. At room temperatures and conventional strain rates, holocrystalline igneous rocks are not known to exhibit ductile behavior up to confining pressures of at least 5 GPa.[14] Microscopically, the most pronounced difference between the two rocks was the far greater occurrence and extent of transgranular fracturing in the granodiorite. The clay and cement matrix appears to play a crucial role in both the mechanical and structural response of the graywacke sandstone to stress, facilitating cataclastic flow of grains and effectively damping out transgranular fracturing beyond a grain diameter.

In summary, Rio Blanco graywacke sandstone in the unstressed state can be described as a two-part system with large, strong, nonporous clasts connected by a dense and intricate network of small, weak clay and matrix minerals. The pore network of the rock consists of the open areas in the cement matrix, with pore diameters

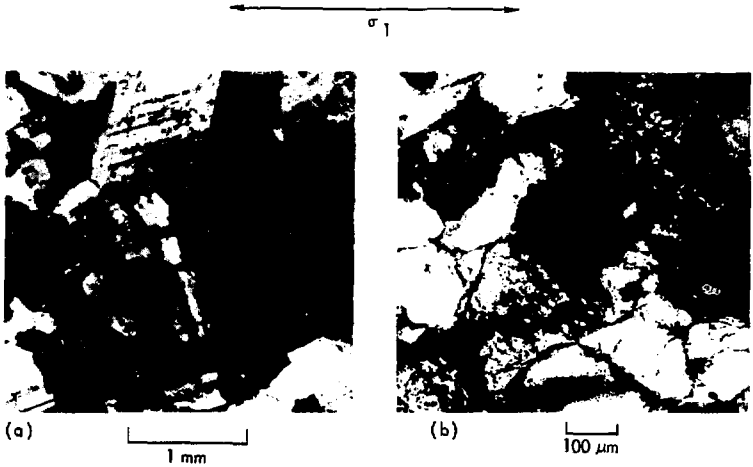

Fig. 27. Comparison of a holocrystalline igneous rock and a clastic sedimentary rock tested to failure under similar conditions of uniaxial stress (300 MPa confining pressure). Both specimens were taken from a region away from the shear zone. (a) Sample P16 of Piledriver granodiorite: note the extent of transgranular fractures. (b) (b) Sample RB 11 of Rio Blanco graywacke sandstone: transgranular fractures are rare and short.

less than 10 μm. The low gas permeability of this sandstone is probably due to the small pore size and the intricacy of the pore networks.

Uniaxial-strain tests caused partial breakdown of the cement structure, narrow grain-boundary cracks, and short transgranular cracks. These effects were observed at maximum strains as low as 1.4%. Increased strain appeared to increase the degree of breakdown, although the effect was not pronounced enough to predict strain regime by the damage observed. The resulting increase in pore size due to cement breakdown is likely to cause some increase in permeability. The transgranular fractures observed probably do not affect permeability, as they were rarely observed to extend further than half a grain diameter and thus could not create new pore networks.

Uniaxial stress is likely to be more effective than uniaxial strain in increasing permeability. In the brittle regime the creation of continuous fault zones with abundant

intergranular fracturing should greatly increase permeability along these zones. Away from the fault zone, the effect of uniaxial stress on permeability is probably similar to that of uniaxial strain. With increased confining pressure, the amount of the sample directly involved in the failure process also increased, as evidenced by the width of the zone of fractured grains and the extent of transgranular fracture away from the failure zone. Whether permeability is increased also (compared to brittle samples) is uncertain. The transgranular fracturing was observed to be limited in length but probably not interconnected, thus not contributing significantly to new pore networks. The shear-zone area of transitional samples could conceivably be less permeable than the same area in brittle samples, where wide grain-boundary cracks predominated. In the ductile regime, all constituents of the rock, clasts and cement matrix, were generally fractured. Transgranular fracturing was extensive in length, likely creating new pore networks. The result may be a significant permeability increase.

The permeability effects discussed above are hypothetical. This study would be greatly aided by quantitative permeability measurements made on stressed samples. The application of these results to the *in situ* response of the same rock to a shock wave is more uncertain. The most extensively fractured sample (and possibly the most permeable) was tested at 600 MPa confining pressure, which is considerably higher than pressures assumed to be relevant at gas-stimulation depths. The strain rates in the laboratory experiments were lower by factors of 10^5 to 10^{10} than shock-wave strain rates. In uniaxial-stress tests on holocrystalline rock, increasing the strain rates raised the failure envelope and enhanced brittle behavior (Schock and Heard[14]). Similarly, the high strain rates caused by a shock wave may favor brittle behavior in sandstone even at depths corresponding to the confining pressures that cause transitional behavior in the laboratory. Quantitative permeability measurements, coupled with careful microscopic studies of laboratory-tested and *in situ* shocked samples, could help to resolve these speculations.

Acknowledgments

I am grateful to R. Schock for his advice and assistance in this project, to L. Luedke and J. Hampel of the University of California, Berkeley, for sample preparation and photographic assistance, and to B. Bonner, A. Duba, H. Heard, and H. Weed. for their comments on this manuscript. The initial part of this work was performed while I was employed through the Chemistry Department Summer Student program. The SEM used in the study is operated by the Electron Microscope Laboratory of the University of California, Berkeley, through NSF Grant GB-38359.

References

1. J. Toman and H. A. Tewes, Project Rio Blanco: Phase I Technical Studies, Lawrence Livermore Laboratory, Rept. UCID-15968 (1972).

2. J. Toman and H. A. Tewes, Project Rio Blanco: Technical Studies II, Lawrence Livermore Laboratory, Rept. UCID-16259 (1973).

3. R. N. Schock, H. C. Heard, and D. R. Stephens, Mechanical Properties of Rocks From the Site of the Rio Blanco Gas Stimulation Experiment, Lawrence Livermore Laboratory, Rept. UCRL-51260 (1972).

4. I. Y. Borg, Microscopic Examination of Undeformed and Laboratory Deformed Wagon Wheel Rocks, Lawrence Livermore Laboratory, Rept. UCRL-51015 (1971).

5. A. Timur, W. B. Hemphkins, and R. M. Weinbrandt, "Scanning Flectron Microscope Study of Pore Systems in Rocks," J. Geophys. Res. 76, 4932-4948 (1971).

6. R. M. Weinbrandt and I. Fatt, "A Scanning Electron Microscope Study of the Pore Structure of Sandstone," J. Pet. Technol., 543-548 (May 1969).

7. F. M. Kieke and D. J. Hartmann, "Detecting Microporosity to Improve Formation Evaluation," J. Pet. Technol., 1080-1086 (October 1974).

8. D. F. Krinsley and S. V. Margolis, "A Study of Quartz Sand Surface Textures with the Scanning Electron Microscope," Trans. N. Y. Acad. Sci. 31, 457-477 (1969).

9. R. Quong, Permeability of Fort Union Formation Sandstone Samples: Project Rio Blanco, Lawrence Livermore Laboratory, Rept. UCID-16182 (1973).

10. G. E. Duvall and G. R. Fowles, "Shock Waves," in High Pressure Physics and Chemistry 2, R. S. Bradley, Ed. (Academic Press, London and New York, 1963), pp. 209-292.

11. D. Griggs and J. Handin, "Observations on Fracture and a Hypothesis of Earthquakes," in Rock Deformation, G.S.A. Memoir 79, D. Griggs and J. Handin, Eds. (Geologic Survey of America, New York, 1960), pp. 347-373.

12. R. N. Schock, H. C. Heard, and D. R. Stephens, "Stress-Strain Behavior of a Granodiorite and Two Graywackes on Compression to 20 Kilobars," J. Geophys. Res. 78, 5922-5941 (1973).

13. I. Borg, M. Friedman, J. Handin, and D. V. Higgs, "Experimental Deformation of St. Peter Sand: A Study of Cataclastic Flow," in Rock Deformation, G.S.A. Memoir 79, D. Griggs and J. Handin, Eds. (Geologic Survey of America, New York, 1960), pp. 133-191.

14. R. N. Schock and H. C. Heard, "Static Mechanical Properties and Shock Loading Response of Granite," J. Geophys. Res. 79, 1662-1666 (1974).

15. W. F. Brace, B. W. Paulding, Jr., and C. Scholz, "Dilatancy and the Fracture of Crystalline Rocks," J. Geophys. Res. 71, 3939-3953 (1966).

16. C. H. Scholz, "Experimental Study of the Fracturing Process in Brittle Rock," J. Geophys. Res. 73, 1447-1454 (1968).

GRS/gw/pf